Available online at www.sciencedirect.com
SCIENCE DIRECT®
Journal of Solid State Chemistry 178 (2005) 1799–1806
JOURNAL OF SOLID STATE CHEMISTRY
www.elsevier.com/locate/jssc

Hydrogen cycling induced diffraction peak broadening in *C*14 and *C*15 Laves phases

V. Iosub[a], J.-M. Joubert[a,*], M. Latroche[a], R. Cerný[b], A. Percheron-Guégan[a]

[a]*Laboratoire de Chimie Métallurgique des Terres Rares, ISCSA, CNRS, 2-8 rue Henri Dunant, F-94320, Thiais Cedex, France*
[b]*Laboratoire de Cristallographie, Université de Genève, 24 Quai E. Ansermet, CH-1211 Genève 4, Switzerland*

Received 10 January 2005; received in revised form 4 March 2005; accepted 11 March 2005
Available online 9 April 2005

Abstract

The diffraction peak broadening induced by hydrogen absorption–desorption cycling has been analyzed in four different Laves phase compounds with the *C*14 and *C*15 structures. The broadening is due to strain most probably originating from dislocations generated at the interface between the α and β hydride phases in connection with the cell volume difference between the two phases. It has been shown that it is strongly compound dependent. In the case of the *C*14 structure, the broadening is large and isotropic, and the latter can be related to the isotropy of the elastic constants of the metallic phase. The broadening is less for the compounds with the *C*15 structure, which can be related to a possibly softer lattice. Better ageing properties after long-term cycling are predicted for this crystal structure.

Keywords: Metal hydrides; Hydrogen storage; Laves phases; *C*14; *C*15; Line broadening; Synchrotron radiation

1. Introduction

Hydride-forming intermetallic compounds are of interest for a number of applications ranging from hydrogen gas storage [1–3] to nickel–metal hydride batteries [4,5]. Extensive absorption–desorption cycling may affect drastically the properties such as absorption and desorption pressures, plateau slope or hydrogen storage capacity [6–10]. Therefore, the ageing behavior is a key parameter to govern to develop long-term applications.

It has been shown in previous work that a large broadening of the diffraction peaks in the early cycles of the hydrogenation due to the formation of lattice defects such as dislocations may result after prolonged cycling in a significant decrease of the capacity, related to a progressive disproportionation of the compound [8]. Following the work of Wu et al. [11,12] on the binary compound $LaNi_5$, we have performed an extensive study of the diffraction peak broadening of a series of hydrogen-cycled compounds $LaNi_{5-x}M_x$ (M = Ni, Mn, Al, Co, Cu, Fe, Sn) [13,14]. It has been shown that the peak broadening observed in these compounds can be exclusively attributed to strains produced by the presence of a high density of dislocations. Those dislocations originate from the large misfit of the lattice parameters in the two-phase domain between the α (hydrogen-poor solid solution) and the β (hydrogen-rich hydride) phases. Indeed, the volume difference may reach 22% in the case of $LaNi_5$.

Besides the AB_5 intermetallic compounds (hexagonal, $CaCu_5$ type; A = rare earths, $B = d$ or p elements), another well-known family of hydride-forming compounds are the so-called AB_2 compounds (A = Zr, Ti; B = Ni, V, Cr, Mn) (for a review see, e.g., Refs. [4,15,16]). These compounds are Laves phases crystallizing either in the *C*14 (hexagonal, $MgZn_2$ type) or *C*15 structure (cubic, $MgCu_2$ type). Hydrogen locates in these two structures in interstitial tetrahedral sites.

*Corresponding author. Fax: +33 1 49 78 12 03.
E-mail address: jean-marc.joubert@glvt-cnrs.fr (J.-M. Joubert).

0022-4596/$ - see front matter © 2005 Elsevier Inc. All rights reserved.
doi:10.1016/j.jssc.2005.03.018

We present hereafter results of the peak broadening study after hydrogen cycling of Laves phases by means of synchrotron powder diffraction. The results allow a comparison between $C14$ and $C15$-type compounds, a preliminary study of the effect of the metal composition and a comparison between AB_5 and AB_2-type compounds.

2. Experimental

The intermetallic compounds were synthesized by melting of the pure elements in an induction cold crucible furnace under argon atmosphere. They were subsequently wrapped in a tantalum foil and annealed in a silica tube sealed under argon atmosphere at 1000–1050 °C during 7 days. A study of phase diagrams shows that it is quite common for Laves phases that an increase of the Ni content is accompanied by a decrease of the Zr content [17]. To be synthesized as single phases and to avoid the precipitation of Zr–Ni phases, one must increase the stoichiometric ratio B/A over 2 yielding the so-called non-stoichiometric compounds. In our case the ratio $B/A = 2.15$ was chosen for the Ni-rich compounds. The samples were characterized by conventional X-ray diffraction, optical metallography and electron probe microanalysis (EPMA). The measurement of the thermodynamic properties of the hydrides was performed at 75 °C (hydrogen capacity, absorption and desorption plateau pressures) with a so-called volumetric device using the Sievert's method. The same apparatus was used to charge each sample after activation to half of its capacity, allowing a conventional X-ray diffraction measurement in order to determine the lattice parameters of the saturated α and under-saturated β phases in equilibrium. Fifteen absorption–desorption cycles were performed between 10 bar and vacuum at a constant temperature (25 °C during five activation cycles, 75 °C during the last 10 cycles). Due to a difficult activation and cycling behavior, sample S3 (see Table 1) was submitted to only nine cycles and to pressures up to 100 bar. After cycling, the powdered samples were examined by scanning electron microscopy (SEM). The average particle size after hydrogen decrepitation was estimated visually from the images.

The powder diffraction synchrotron measurements of the non-cycled and cycled compounds were performed at the Swiss Norwegian Beamline at the ESRF, Grenoble, France in the conventional Debye–Scherrer geometry (capillary diameter 0.3 mm, step scan, 2θ range 6–47°, step size 0.005° 2θ, time per step 2 s). The diffractometer was equipped with six detectors with Si (111) analyzers. Very particular care was taken regarding the choice of the wavelength. The major concern was about the compound $ZrMn_{0.71}Ni_{1.21}V_{0.22}$ with the $C15$ structure. In addition to the evidencing of broadening, one of the major issues of the experiment was to determine if the broadening is isotropic or not. For this purpose, one must be able to evaluate the peak widths of the Miller indices families like $h\,0\,0$, $h\,h\,0$, $h\,h\,h$. Among these families, $h\,0\,0$ peaks are peculiarly relevant. However, due to the systematic extinctions in the space group $Fd\bar{3}m$, only the peaks 400 and 800 are present in the diagram. Moreover, the 400 reflection intensity is very weak when measured at Cu$K\alpha$ wavelength and prevents any study of the angle dependence of $h\,0\,0$ family. This is due to the structure factor of this reflection (proportional to $2f_{16d}-f_{8a}$) and to the peculiar values of the site scattering factor f_{16d} given the atoms occupying site 16d (Mn, Ni and V) which nearly equals half the value of $f_{8a} = f_{Zr}$. A modification of one of the site scattering f factors can be achieved when exploring the effect of the resonant scattering by adjusting the wavelength close to the absorption edge of one atom occupying either the site 16d or 8a. We have chosen the X-ray energy 20 eV below Zr K edge. This allows benefiting from the anomalous dispersion correction $f'_{Zr} = -6.3e$ raising the 400 peak intensity from 0.7% to 2.8% of the main peak and thus allowing its measurement. The exact value of the wavelength ($\lambda = 0.68957$ Å) was calibrated with the NIST silicon standard SRM 640b.

The analysis of the peak widths was performed by an individual profile fitting using the software EVA [18]. A symmetrical Voigt function was used for each peak and the contributions in terms of Gaussian and Lorentzian peak widths were obtained. The instrumental contribution to the broadening was measured by using the NIST LaB_6 standard SRM 660. The deconvolution was performed according to the method of Langford [19,20] and the sample integral breadths (β in units of 2θ) were obtained. They are plotted in the form of a conventional Williamson–Hall plot [21] and the average strain (e) may be obtained from the slope of the linear fit ($\beta\cos\theta/\lambda$ vs. $\sin\theta$)

$$\frac{\beta\cos\theta}{\lambda} = \frac{4e\sin\theta}{\lambda} + 1/D, \tag{1}$$

where D is the apparent coherent domain size.

In addition, a conventional Rietveld analysis was performed (program Fullprof [22]) allowing precise lattice parameter determination and choosing between a substitutional and a vacancy model in the case of the non-stoichiometric $C15$ structures. These results were compared to measurements of the mass density using a gas pycnometer Accupyc 1330.

3. Results

The main phase in the four studied samples (compositions in Table 1) has the crystal structure types $C14$ for

Table 1
Metallurgical characterization of the samples

Sample	Nominal composition	Analyzed composition	Crystal structure	Phase content (wt%)	Lattice parameters		
					a (Å)	c (Å)	V (Å^3)
S1	$Zr_{0.8}Ti_{0.2}MnNi_{0.8}V_{0.2}$ (AB_2)	$Zr_{0.80(1)}Ti_{0.20(1)}Mn_{0.97(2)}Ni_{0.78(2)}V_{0.21(1)}$ ($AB_{1.96}$)	$C14$	100	4.995(1)	8.153(1)	176.17(4)
S2	$Zr_{0.8}Ti_{0.2}Mn_{0.9}Ni_{0.8}V_{0.3}$ (AB_2)	$Zr_{0.80(1)}Ti_{0.20(1)}Mn_{0.89(1)}Ni_{0.77(1)}V_{0.32(1)}$ ($AB_{1.98}$)	$C14$	100	5.001(1)	8.165(1)	176.85(4)
S3	$Zr_{0.8}Ti_{0.2}Mn_{0.72}Ni_{1.21}V_{0.22}$ ($AB_{2.15}$)	$Zr_{0.80(1)}Ti_{0.20(1)}Mn_{0.70(1)}Ni_{1.18(1)}V_{0.28(2)}$ ($AB_{2.16}$)	$C15$	96(1)	7.023(1)		346.37(5)
		Additional phase not analyzed	$C14$	4(1)	4.975(1)	8.111(1)	173.86(4)
S4	$ZrMn_{0.72}Ni_{1.21}V_{0.22}$ ($AB_{2.15}$)	$ZrMn_{0.77(3)}Ni_{1.28(5)}V_{0.24(2)}$ ($AB_{2.29}$)	$C15$	99(1)	7.070(1)		353.36(5)
		$ZrNi_{1.42(1)}Mn_{0.09(1)}V_{0.01(1)}$ ($A_7B_{10.64}$)	Zr_7Ni_{10}	1(1)			

The nominal and analyzed (EPMA) compositions, the crystal structure, the phase content (Rietveld analysis) and the lattice parameters are indicated.

Table 2
Description of the stoichiometric $C14$ and $C15$ phases (A = Zr, Ti; B = Mn, Ni, V)

Strukturbericht	Structure type	Space group	Atomic positions
$C14$	$MgZn_2$	$P6_3/mmc$	A in 4f (1/3, 2/3, $z = 1/16$) B in 2a (0, 0, 0) B in 6h ($x = 5/6$, $2x$, 1/4)
$C15$	$MgCu_2$	$Fd\bar{3}m$ (centrosymmetric description)	A in 8a (1/8, 1/8, 1/8) B in 16d (1/2, 1/2, 1/2)

Ni-poor and $C15$ for Ni-rich samples (see Table 2 for a description of the structural features of these two structures). Sample S3 presents a small amount (4 wt%) of the $C14$ phase. Traces of the Zr_7Ni_{10} phase were also apparent in the sample S4. The two other samples were single phase. The microprobe analysis yielded compositions in agreement with the nominal composition except for sample S4 for which a stoichiometric ratio $B/A = 2.29$ was measured and explains the precipitation of the Zr_7Ni_{10} phase. These results are reported in Table 1, together with measured lattice parameters. The two samples with the $C15$ structure deviate from the ideal stoichiometry $B/A = 2$ corresponding to full occupancy of site 8a by Zr or Ti only, and full occupancy of site 16d by V, Mn and Ni. The way the non-stoichiometry is accounted for in the crystal structure has been investigated by the structural refinement using measured powder diffraction data and by mass density measurement. Basically, two models could explain the A atoms deficiency, i.e., A vacancies or substitution of B atoms on the A sublattice (V was supposed to substitute Zr due to closer electronic properties). The results are reported in Table 3 and are in favor of a substitution model in both cases.

Observed hydrogen storage capacity ranges between 0.75 and $1H/M$ depending on the compounds. No significant decrease of the hydrogen capacity was noticed during cycling. The lattice parameters of the α and β hydride phases in equilibrium and the calculated lattice expansion are presented in Table 4. One may note that the discrete volume expansion varies between 11.9% and 20.8%. For the hexagonal structure, one may notice the high isotropy of the lattice expansion.

The measured hysteresis (H, logarithm of the ratio of the absorption and desorption pressures) as well as the average particle size after cycling (G) are also presented in Table 4. Larger grain size and low hysteresis are

Table 3
Non-stoichiometry models for the samples with the *C*15 structure

Sample	*B*/*A* (measured EPMA)	Density (measured pycnometry)	Substitutional model		Vacancy model	
			B/*A* (refined)	Density (calculated)	*B*/*A* (refined)	Density (calculated)
S3	2.16	7.49(1)	2.33 $(Zr_{0.72}Ti_{0.18}V_{0.1})(Mn_{0.68}Ni_{1.15}V_{0.17})$	7.46 $(Zr_{0.76}Ti_{0.19}V_{0.05})(Mn_{0.67}Ni_{1.12}V_{0.22})$ $AB_{2.16}$	2.06 $(Zr_{0.78}Ti_{0.19}\square_{0.03})(Mn_{0.65}Ni_{1.09}V_{0.26})$	7.26 $(Zr_{0.74}Ti_{0.19}\square_{0.08})(Mn_{0.65}Ni_{1.09}V_{0.26})$ $AB_{2.16}$
S4	2.29	7.64(1)	2.21 $(Zr_{0.94}V_{0.07})(Mn_{0.70}Ni_{1.17}V_{0.14})$	7.58 $(Zr_{0.91}V_{0.09})(Mn_{0.70}Ni_{1.17}V_{0.13})$ $AB_{2.29}$	2.06 $(Zr_{0.97}\square_{0.03})(Mn_{0.67}Ni_{1.12}V_{0.21})$	7.25 $(Zr_{0.87}\square_{0.13})(Mn_{0.67}Ni_{1.12}V_{0.21})$ $AB_{2.29}$

Stoichiometric ratio and mass density measured by EPMA and pycnometric measurements are compared with the same parameters refined from Rietveld refinement or calculated to match the stoichiometry in a substititutional model (V substitutes on site 8*a*) and a vacancy model (vacancy on site 8*a*).

Table 4
Lattice parameters of α and β phases in equilibrium, lattice expansions relative to the α phase, hysteresis ($H = \ln P_{abs}/P_{des}$), estimated average particle size after cycling (G, SEM), average strain (e) for cycled and non-cycled compounds

Sample	Saturated α phase			Undersaturated β phase			Relative discrete lattice expansion			H	G (μm)	e_{cycled} (%)	$e_{non\text{-}cycled}$ (%)	$e_{cycled}-e_{non\text{-}cycled}$ (%)
	a (Å)	c (Å)	V (Å^3)	a (Å)	c (Å)	V (Å^3)	$\Delta a/a$ (%)	$\Delta c/c$ (%)	$\Delta V/V$ (%)					
S1	5.007(1)	8.175(1)	177.5(1)	5.331(1)	8.708(1)	214.4(1)	6.5	6.5	20.8	0.7(1)	6(3)	0.192(7)	0.046(4)	0.146
S2	5.021(1)	8.200(1)	179.0(1)	5.309(1)	8.676(1)	211.8(1)	5.7	5.8	18.3	0.20(5)	9(3)	0.119(6)	0.036(4)	0.083
S3	7.097(1)	—	357.5(1)	7.370(1)	—	400.2(1)	3.8	—	11.9	0.20(5)	20(3)	0.061(4)	0.045(4)	0.016
S4	7.087(1)	—	355.9(1)	7.512(1)	—	423.9(1)	6.0	—	19.1	0.10(5)	12(3)	0.094(4)	0.079(4)	0.015

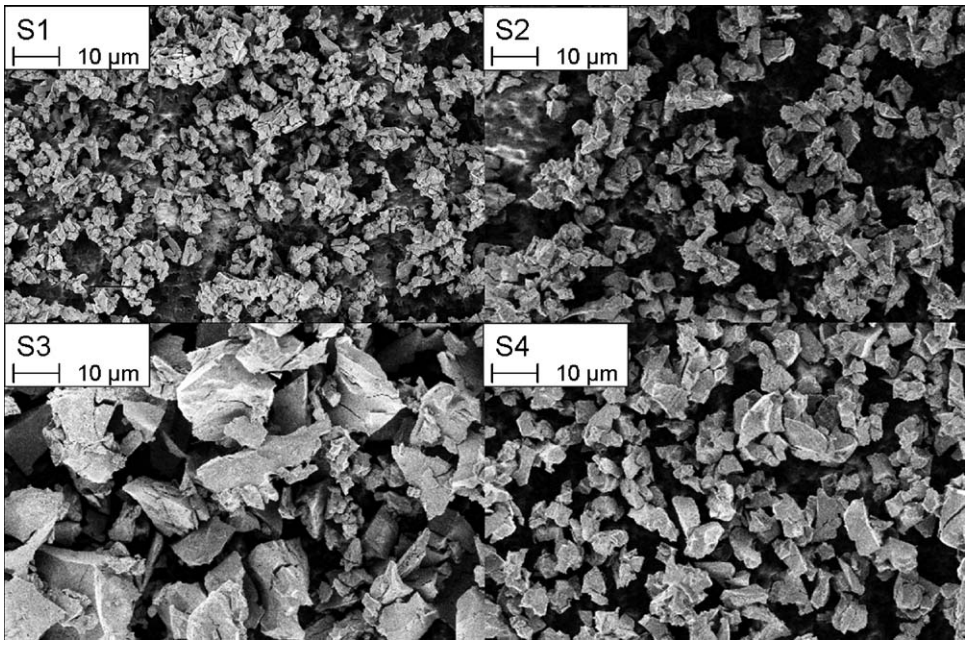

Fig. 1. Selected SEM images of the four samples after hydrogen cycling.

observed for the compounds adopting the *C*15 structure. Selected SEM images are presented in Fig. 1.

As an example, selected parts of the measured synchrotron powder diffraction diagrams of cycled and non-cycled S1 sample are compared in Fig. 2. The conventional Williamson–Hall plots are presented in Fig. 3. The peak widths of the non-cycled compounds are typical for intermetallic compounds and related to the homogeneity of the composition and to the presence of intrinsic structural defects introduced during the crushing procedure for example. Wider peaks are observed for sample S4 which can be related to the higher inhomogeneity of Ni concentration evidenced by the EPMA. An evaluation of the absolute broadening of the cycled compounds is hindered by the non-negligible natural broadening of the non-cycled compounds. Therefore, the evaluation of the hydrogen-induced broadening must be done by comparison, for each sample, between cycled and non-cycled compounds. This analysis shows a significant change of the broadening for the two compounds with the *C*14 structure (sample S1 presenting a larger change of the broadening than S2), while the change of the broadening is weak in the two compounds with the *C*15 structure. In each case, the broadening is observed to be isotropic. The intersect of the regression lines with the *y*-axis shows that the size broadening is always minor and that only strain broadening is of importance. The value of the average strain (e) is reported for each cycled and non-cycled compound in Table 4.

4. Discussion

The studied compositions of the Laves phases were chosen in the frame of hydrogen gas storage alloy development. They were calculated in order to give rise to hydride formation under approximately 3 bar at 75 °C. They all derive from the binary compound $ZrMn_2$ (*C*14) by appropriate substitution on the Zr and Mn sublattices in order to raise the absorption pressure. The two compounds $Zr_{0.8}Ti_{0.2}MnNi_{0.8}V_{0.2}$ (S1) and $Zr_{0.8}Ti_{0.2}Mn_{0.9}Ni_{0.8}V_{0.3}$ (S2) with the *C*14 structure allow studying the effect of a small variation in the vanadium concentration. By increasing the average *d*-electron concentration, one may switch from the *C*14 to the *C*15 structure [23]. This was done for the samples $Zr_{0.8}Ti_{0.2}Mn_{0.72}Ni_{1.21}V_{0.22}$ (S3) and $ZrMn_{0.72}Ni_{1.21}V_{0.22}$ (S4) by increasing the nickel content. For the two latter samples the effect of titanium content can be studied.

The compounds with the *C*15 structure have been shown to be non-stoichiometric. This is in agreement with previous findings in other systems and seems to be correlated with the nickel substitution [17]. The present results are in favor of a substitution model (*B* atom, most probably V, substituting on the Zr (Ti) site). This is found to be in agreement with the model described to explain the non-stoichiometry in $HfCo_2$ [24].

The differences of strain between the cycled and non-cycled compounds can be related neither to a remaining presence of hydrogen nor to additional local variations of the composition since the homogeneity is unlikely to

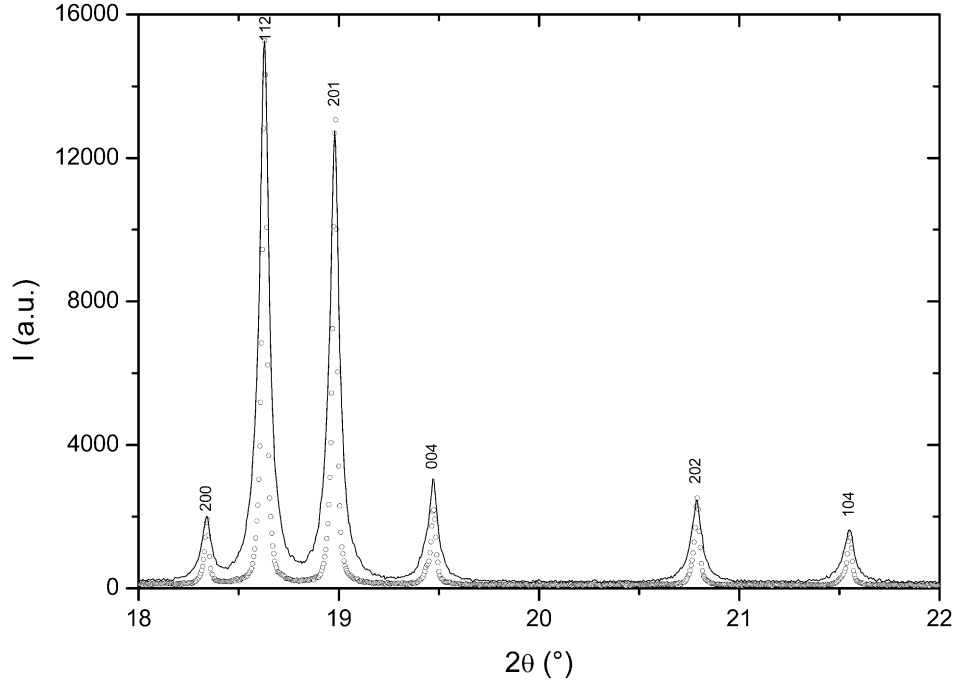

Fig. 2. Selected parts of the diffraction diagrams of sample S1 cycled (full lines) and non-cycled (dots).

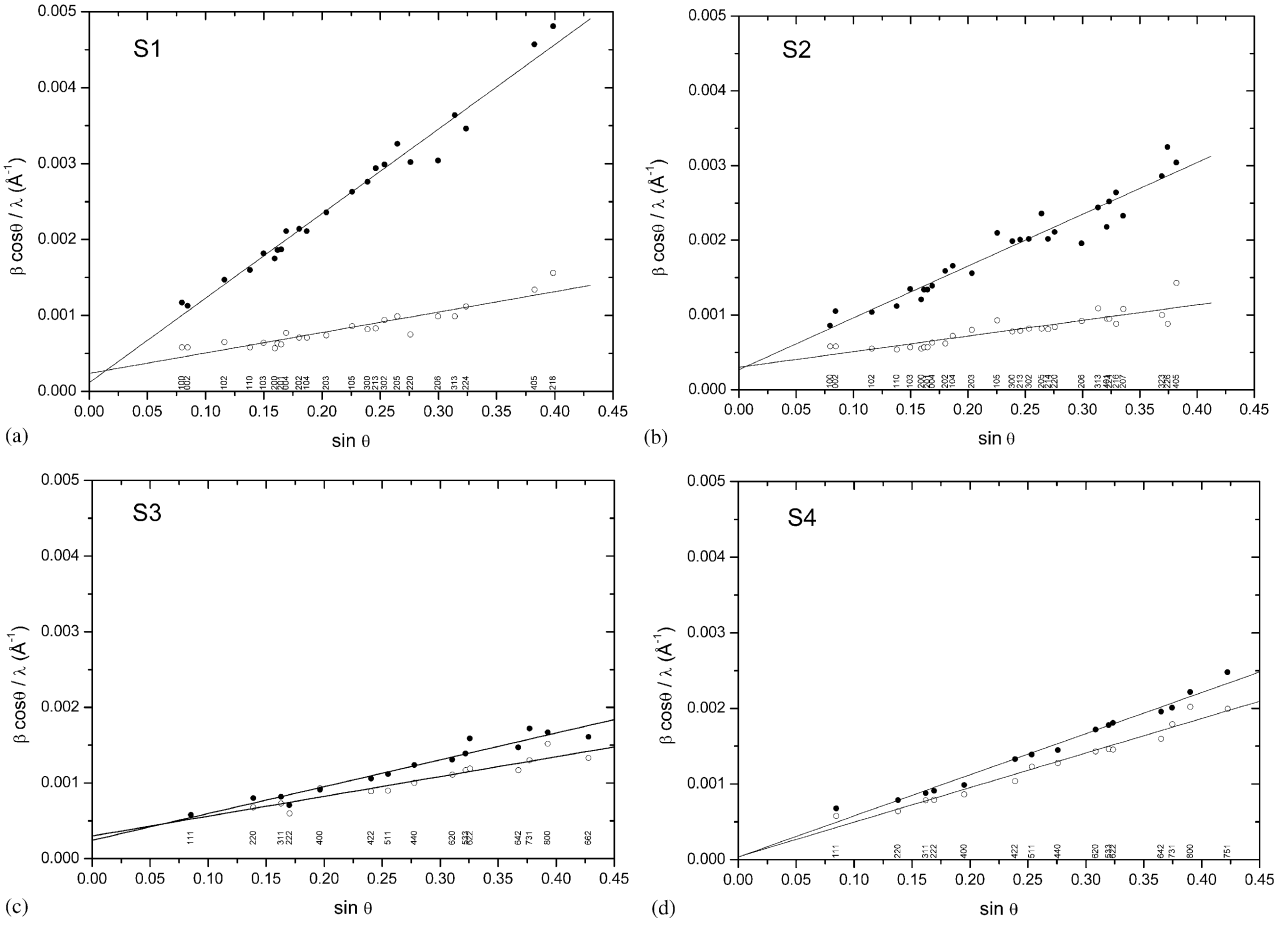

Fig. 3. Williamson–Hall plot for the four samples in cycled (solid symbols) and non-cycled (open symbols) states (*a*: S1, *b*: S2, *c*: S3, *d*: S4). The maximum relative error on the line widths measured for the sample weakest lines is 6%.

change during cycling. Most probable explanation for the strain increase with the cycling is therefore the presence of dislocations as evidenced in $LaNi_5$ compound and derivatives [11–13]. In the following, the term strain for a given sample should be understood in terms of strain increase.

Between the two samples with the *C*14 structure (S1 and S2), the higher amount of strains, the larger hysteresis and the stronger decrepitation of sample S1 may be related to the higher volume expansion observed in this sample. One may attribute the differences to the changes of vanadium content. Indeed, this element has been described in the literature as beneficial at least for the hysteresis [25,26]. Concerning the samples with the *C*15 structure, hysteresis and strain are already low in S4. Reduction of the discrete lattice expansion related to Ti substitution for Zr in S3, has a significant effect only on reducing the decrepitation.

Larger strains are observed in the samples with the *C*14 structure than in the samples with the *C*15 structure where they are nearly absent. This phenomenon cannot be accounted for by differences in the lattice expansion during hydrogenation since sample S4 has a volume expansion between those of S1 and S2. This may indicate that the difference in behavior is mainly structural. In $Zr(Al_xFe_{1-x})_2$ system, a rare example for which the elastic properties of the *C*14 and *C*15 phases could be compared at an equivalent composition, it has been shown that the *C*14 phase has a higher bulk modulus than the *C*15 phase [27]. This observation, provided that it could be transposed to our system, is in line with our observation in the case of $LaNi_5$ substituted compounds that a lower bulk modulus is associated with more resistant compounds to the defect formation [28]. One may predict from the lower hydrogen cycling induced strains observed with the *C*15 structure a better long-term ageing in the frame of a hydrogen storage application, as is observed for $LaNi_5$ derivatives [8].

$LaNi_5$ presents after hydrogenation cycling a huge and highly anisotropic peak broadening. The peaks with $hk0$ indices are extensively broadened while those with $00l$ indices are nearly un-broadened. Previous study based on the model of Refs. [29,30] has allowed the evidencing of the dislocation system $1/3\langle\bar{2}110\rangle\{0\bar{1}10\}$ as responsible for the broadening [11,12].

In the case of the cycled compounds with the *C*14 structure, the absence of any anisotropy in the broadening has not allowed performing a detailed analysis of the dislocation nature and density since many systems or combinations of systems could account for an isotropic broadening. One may however compare the average strains which reach 0.72% along $h00$ for $LaNi_5$ [13] a value significantly higher than the one obtained in sample S1.

The fact that the broadening is highly anisotropic in $LaNi_5$ is related to the fact that one main dislocation system is activated introducing highly anisotropic strains. The absence of anisotropy in the *C*14 structure may be explained by an isotropic distribution of different dislocation systems. Indeed, no anisotropy was observed in the lattice expansion of *C*14 structure contrary to what is observed in the case of $LaNi_5$ and substituted derivatives for which it is weak but significant (e.g., for $LaNi_5$: $\Delta a/a = 7.3\%$, $\Delta c/c = 6.3\%$).

Finally, the Laves phases are topologically close packed phases (Frank–Kasper phases). The difference between the cubic *C*15 and hexagonal *C*14 structures originates only from a difference in Frank–Kasper polyhedra stacking. In addition, the atoms are arranged as interpenetrating networks with no evidence of directional interactions. Therefore, the anisotropy should be weak even for the *C*14 structure contrary to what occurs in the $CaCu_5$ structure which is not a topologically close packed structure. Indeed, when they have been measured, the elastic constants have been shown to be fairly isotropic in the *C*14 structure (e.g., $CaMg_2$ [31] and $MgZn_2$ [32]). This contrasts with what is observed in the case of $LaNi_5$ for which a high anisotropy of the elastic constants has been evidenced [28,33].

5. Conclusion

This work presents, to our knowledge, the first study of the hydrogen cycling induced peak broadening in Laves phase compounds. It has been shown that the compounds with a *C*14 structure present a significant and isotropic broadening. On the contrary, the broadening is much reduced in the case of the *C*15 structure. This allows predicting a better long-term cycling stability for the latter compounds. As in the case of the AB_5 compounds, the lattice expansion cannot alone explain the different behaviors observed, and one must take into account the elastic properties of the compounds.

Acknowledgment

The authors wish to acknowledge Mrs. Briaucourt and Mrs. Lalanne for help with the sample synthesis and characterization, Mr. Leroy for the EPMA analysis, Mr. Pastol for the help with the SEM examination and the staff of the Swiss Norwegian Beamline at the ESRF (particularly H. Emerich).

References

[1] G.D. Sandrock, J. Alloys Compd. 293–295 (1999) 877–888.
[2] R.C. Bowman Jr., B. Fultz, MRS Bull. 27 (9) (2002) 688–693.
[3] P. Dantzer, Mater. Sci. Eng. A 329-331 (2002) 313–320.

[4] F. Cuevas, J.-M. Joubert, M. Latroche, A. Percheron-Guégan, Appl. Phys. A 72 (2001) 225–238.
[5] J.-M. Joubert, M. Latroche, A. Percheron-Guégan, MRS Bull. 27 (9) (2002) 694–698.
[6] S.W. Lambert, D. Chandra, W.N. Cathey, F.E. Lynch, R.C. Bowman Jr., J. Alloys Compd. 187 (1992) 113–135.
[7] Y. Josephy, E. Bershadsky, M. Ron, J. Less-Common Met. 172-174 (1991) 997–1008.
[8] R.C. Bowman Jr., C.H. Luo, C.C. Ahn, C.K. Witham, B. Fultz, J. Alloys Compd. 217 (1995) 185–192.
[9] G. Friedlmeier, A. Manthey, M. Wanner, M. Groll, J. Alloys Compd. 231 (1–2) (1995) 880–887.
[10] M. Wanner, G. Friedlmeier, G. Hoffmann, M. Groll, J. Alloys Compd. 253-254 (1997) 692–697.
[11] E. Wu, E. Mac. A. Gray, E.H. Kisi, J. Appl. Crystallogr. 31 (1998) 356–362.
[12] E. Wu, E.H. Kisi, E.M.A. Gray, J. Appl. Crystallogr. 31 (1998) 363–368.
[13] R. Cerný, J.-M. Joubert, M. Latroche, A. Percheron-Guégan, K. Yvon, J. Appl. Crystallogr. 33 (2000) 997–1005.
[14] R. Cerný, J.-M. Joubert, M. Latroche, A. Percheron-Guégan, K. Yvon, J. Appl. Crystallogr. 35 (2002) 288.
[15] D.-M. Kim, K.-J. Liang, J.-Y. Lee, J. Alloys Compd. 293–295 (1999) 583–592.
[16] A. Züttel, Materials Today, September (2003) 24–33.
[17] J.-M. Joubert, M. Latroche, A. Percheron-Guégan, I. Ansara, J. Phase Equilib. 16 (6) (1995) 485–492.
[18] J. Nusinovici, DIFFRACplus Search/Match V9.0, Socabim, 2003.
[19] J.I. Langford, J. Appl. Crystallogr. 11 (1978) 10–14.
[20] T.H. Keijser, J. Appl. Crystallogr. 15 (308–314) (1982).
[21] G.K. Williamson, W.H. Hall, Acta Metall. 1 (1) (1953) 22–31.
[22] J. Rodríguez-Carvajal, Proceedings of the XV Congress of Int. Union of Crystallography, Satellite Meeting on Powder Diffraction, Toulouse, France, 1990, p. 127.
[23] O. Bernauer, J. Töpler, D. Noréus, R. Hempelmann, D. Richter, Int. J. Hydrogen Energy 14 (3) (1989) 187–200.
[24] K.C. Chen, E.J. Peterson, D.J. Thoma, Intermetallics 9 (2001) 771–783.
[25] Y.-S. Hsu, T.-P. Perng, J. Alloys Compd. 227 (1995) 180–185.
[26] Y.-S. Hsu, S.-L. Chiou, T.-P. Perng, J. Alloys Compd. 313 (1–2) (2000) 263–268.
[27] F. Willis, R.G. Leisure, I. Jacob, Phys. Rev. B 50 (18) (1994) 13792–13794.
[28] J.-M. Joubert, R. Cerny, M. Latroche, A. Percheron-Guegan, K. Yvon, Intermetallics 13 (2004) 227–231.
[29] P. Klimanek, R. Kuzel Jr., J. Appl. Crystallogr. 21 (1988) 59–66.
[30] R. Kuzel Jr., P. Klimanek, J. Appl. Crystallogr. 21 (1988) 363–368.
[31] A. Sumer, J.F. Smith, J. Appl. Phys. 33 (7) (1962) 2283–2286.
[32] G.W. Shanette, J.F. Smith, Scr. Metall. 3 (1969) 33–36.
[33] K. Tanaka, S. Okazaki, T. Ichitsubo, T. Yamamoto, H. Inui, M. Yamaguchi, M. Koiwa, Intermetallics 8 (2000) 613–618.